

# From Sumatra 2004 to Tohoku-Oki 2011: The systematic GPS detection of the ionospheric signature induced by tsunamigenic earthquakes

Giovanni Occhipinti,<sup>1</sup> Lucie Rolland,<sup>2</sup> Philippe Lognonné,<sup>1</sup> and Shingo Watada<sup>3</sup>

Received 14 September 2012; revised 3 May 2013; accepted 6 May 2013.

[1] The recent tsunamigenic earthquake in Tohoku (11 March 2011) strongly affirms, one more time after the Sumatra event (26 December 2004), the necessity to open new paradigms in oceanic monitoring. Detection of ionospheric anomalies following the Sumatra tsunami demonstrated that ionosphere is sensitive to the tsunami propagation. Observations supported by modeling proved that tsunamigenic ionospheric anomalies are deterministic and reproducible by numerical modeling via the ocean/neutral-atmosphere/ionosphere coupling mechanism. In essence, tsunami induces internal gravity waves propagating within the neutral atmosphere and detectable in the ionosphere. Most of the ionospheric anomalies produced by tsunamis were observed in the far field where the tsunami signature in the ionosphere is clearly identifiable. In this work, we highlight the early signature in the ionosphere produced by tsunamigenic earthquakes and observed by GPS, measuring the total electron content, close to the epicenter. We focus on the first hour after the seismic rupture. We demonstrate that acoustic-gravity waves generated at the epicenter by the direct vertical displacement of the source rupture and the gravity wave coupled with the tsunami can be discriminated with theoretical support. We illustrate the systematic nature of those perturbations showing several observations: nominally the ionospheric perturbation following the tsunamigenic earthquakes in Sumatra on 26 December 2004 and 12 September 2007; in Chile on 14 November 2007; in Samoa on 29 September 2009; and the recent catastrophic Tohoku-Oki event on 11 March 2011. Based on the analytical description, we provide tracks for further modeling efforts and clues for the interpretation of complex—and thus often misleading—observations. The routine detection of the early ionospheric anomalies following the rupture highlights the role of ionospheric sounding in the future ocean monitoring and tsunami detection.

**Citation:** Occhipinti, G., L. Rolland, P. Lognonné, and S. Watada (2013), From Sumatra 2004 to Tohoku-Oki 2011: The systematic GPS detection of the ionospheric signature induced by tsunamigenic earthquakes, *J. Geophys. Res. Space Physics*, 118, doi:10.1002/jgra.50322.

## 1. Introduction

[2] After the Great Sumatra Earthquake and the consequent Indian Ocean Tsunami, scientific community puts the attention to alternative methods in ocean monitoring to improve the response of the tsunami warning systems.

[3] Improvement of classic techniques, as the seismic source estimation [e.g., Ammon *et al.*, 2006] and densification of number of buoys over the oceans [Gonzalez *et al.*, 2005], was supported by a new effort in remote sensing: nominally the

space altimetry observation of the tsunami in the open sea [Okal *et al.*, 1999; Smith *et al.*, 2005] and the tsunami detection by ionospheric monitoring [e.g., Occhipinti *et al.*, 2006].

[4] Today the catastrophic event linked to the Tohoku earthquake and the consequent tsunami declares, one more time, the importance to go forward in this direction. This event validates additionally the detection possibility by optical remote sensing observation of the tsunami impact to the shorelines [Marghany and Hashim, 2011]; it also validates once more the ionospheric observations during the tsunami generation at the epicenter [Rolland *et al.*, 2011b; Tsugawa *et al.*, 2011] as well as its propagation in the open ocean where detections are performed not only by GPS but also, for the first time, by airglow detection [Makela *et al.*, 2011; Occhipinti *et al.*, 2011].

[5] The indirect tsunami observation by ionospheric sounding is based on the idea anticipated in the past by Hines [1972] and Peltier and Hines [1976] that tsunamis produce internal gravity waves (IGWs) in the overlooking atmosphere. During the upward propagation, the IGWs are strongly amplified by the effect of the exponential decrease

<sup>1</sup>Institut de Physique du Globe de Paris, Sorbonne Paris Cité, Université Paris Diderot, France.

<sup>2</sup>Géoazur, Observatoire de la Côte d'Azur, Université de Nice, France.

<sup>3</sup>Earthquake Research Institute, University of Tokyo, Japan.

Corresponding author: G. Occhipinti, Institut de Physique du Globe de Paris, Sorbonne Paris Cité, Université Paris Diderot, France. (ninto@ipgp.fr)

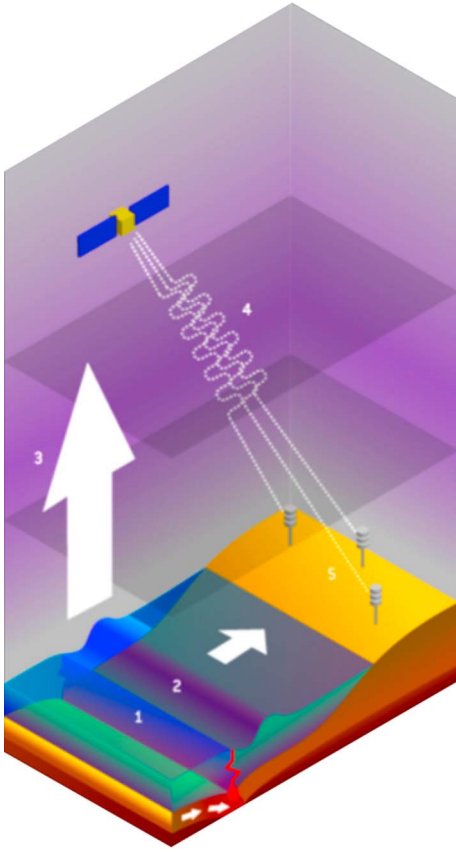


**Figure 1.** Schematic view of the coupling mechanism and the ionospheric sounding by GPS. The vertical displacement of the ground floor (1) produced by an earthquake is directly transferred at the sea surface (2) following the incompressible hypothesis. The sea-surface displacement initiates an internal gravity wave (IGW) propagating into the ocean (tsunami) as well as into the overlooking atmosphere. During the upward propagation the atmospheric IGW interact with the ionospheric plasma (3) creating perturbation in the plasma density and consequently in the local refraction index. The electromagnetic waves emitted by GPS satellites (4) to the ground stations (5) are perturbed by the plasma density variations and are able to image the signature of the IGW in the ionosphere.

of the air density. The interaction of IGWs with the plasma at the ionospheric height produces strong variations in the plasma velocity and plasma density observable by ionospheric sounding (Figure 1).

[6] The encouraging work of *Artru et al.* [2005] based on the total electron content (TEC) observations, performed by the Japanese dense GPS network GEONET, following the peruvian tsunamigenic quake on 23 June 2001 ( $M=8.4$  at 20:33 UT) opens the modern debate about the feasibility of tsunami detection by ionospheric sounding.

[7] In essence, *Artru et al.* [2005] show ionospheric traveling waves reaching the Japanese coast 22 h after the tsunami generation, with an azimuth and arrival time consistent with tsunami propagation. Moreover, a period between 22 and 33 min, consistent with the tsunami, was identified in the observed TEC signals. The tsunami generated IGWs were,

however, superimposed by other signals associated to traveling ionospheric disturbances [*Aframovich et al.*, 2003; *Balthazor and Moffett*, 1997]. The ionospheric noise is large in the gravity domain [*Garcia et al.*, 2005]; consequently, the identification of the tsunami signature in the TEC was ambiguous, and the debate still open.

[8] The giant tsunami following the Sumatra-Andaman event ( $M_w=9.3$ , 0:58:50 UT, 26 December 2004 [*Lay et al.*, 2005]), one order of magnitude larger than the Peruvian tsunami, provided worldwide remote sensing observations in the ionosphere, giving the opportunity to explore ionospheric tsunami detection with a vast data set. In addition to seismic waves detected by global seismic networks [*Park et al.*, 2005]; co-seismic displacement measured by GPS [*Vigny et al.*, 2005]; oceanic sea-surface variations measured by altimetry [*Smith et al.*, 2005]; detection of magnetic anomaly [*Iyemori et al.*, 2005; *Balasis and Manda*, 2007] and acoustic-gravity waves [*Le Pichon et al.*, 2005]; a series of ionospheric disturbances, observed with different techniques, have been reported in the literature [*Liu et al.*, 2006a, 2006b; *Lognonné et al.*, 2006; *DasGupta et al.*, 2006; *Occhipinti et al.*, 2006, 2008b].

[9] Two ionospheric anomalies in the plasma velocities were detected north of the epicenter by a Doppler sounding network in Taiwan [*Liu et al.*, 2006a]. The first was triggered by the vertical displacement induced by Rayleigh waves. The second, arriving 1 h later with a longer period, is interpreted by *Liu et al.* [2006a] as the response of ionospheric plasma to the atmospheric gravity waves generated at the epicenter.

[10] A similarly long period perturbation, with an amplitude of 4 TECU peak to peak, was observed by GPS stations located on the coast of India [*DasGupta et al.*, 2006]. (The TEC is expressed in TECU units (TECU);  $1 \text{ TECU} = 10^{16} e^-/m^2$ ). These perturbations are interpreted by the authors as the ionospheric signature of IGWs coupled at sea level with the tsunami or the atmospheric-gravity waves generated at the epicenter. Comparable TEC observations were done for five GPS stations (12 station-satellite pairs) scattered in the Indian Ocean [*Liu et al.*, 2006b]. The 30 s differential amplitudes are equal to or smaller than 0.4 TECU (which generates amplitudes comparable to the *DasGupta et al.* [2006] observations for periods of  $\approx 165$  min, i.e., 30 points) and the arrival times coherent with the tsunami propagation. The observed satellites were located approximately at the station zenith.

[11] Close to these observations, the Topex/Poseidon and Jason-1 satellites acquired the key observations of the Sumatra tsunami with altimetry profiles. The measured sea level displacement is well explained by tsunami propagation models with realistic bathymetry and provides useful constraints on source mechanism inversions [e.g., *Song et al.*, 2005]. In addition, the inferred TEC data, required to remove the ionospheric effects from the altimetric measurements [*Bilitza et al.*, 1996], showed strong anomalies in the integrated electron density [*Occhipinti et al.*, 2006].

[12] In essence altimetric data from Topex/Poseidon and Jason-1 shows at the same time the tsunami signature on the sea surface and the supposed tsunami signature in the ionosphere.

[13] By a three-dimensional numerical modeling, *Occhipinti et al.* [2006] compute the atmospheric IGWs generated by the Sumatra tsunami and their interaction with the ionospheric plasma. The quantitative approach reproduces the TEC observed by Topex/Poseidon and Jason-1 in the

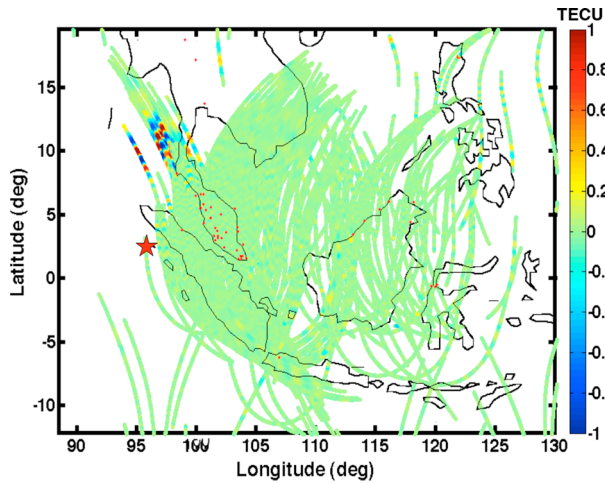


**Figure 2.** Total electron content (TEC) perturbation appearing 15 min after the earthquake in Sumatra (26 December 2004). The ionospheric piercing points (IPPs) obtained by satellites PRN01, 03, 13, 19, 20, and 23 coupled with the SEAMARGES network (red points) are shown here during 1 h and highlight a clear early perturbation moving from the epicenter (the red star) to the North of Sumatra. The signal observed by each satellite is shown on Figure 3 where the time scale is visible.

Indian Ocean the 26 December 2004. Consequently, *Occhipinti et al.* [2006] closed the debate about the nature and the existence of the tsunami signature in the ionosphere. The results obtained by *Occhipinti et al.* [2006] were recently reproduced by *Mai and Kiang* [2009]. Other theoretical works appeared recently to explore the possible detection by airglow monitoring [*Hickey et al.*, 2010] and Over-The-Horizon radar [*Coisson et al.*, 2011], as well as to calculate the effect of dissipation, nominal viscosity, and thermal conduction [*Hickey et al.*, 2009]. Airglow observation during the Tohoku tsunami propagation close to Hawaii [*Makela et al.*, 2011; *Occhipinti et al.*, 2011] validates, for the first time, the airglow detection possibility.

[14] The method developed by *Occhipinti et al.* [2006] is also used to estimate the role of the geomagnetic field in the tsunami signature at the E-region and F-region [*Occhipinti et al.*, 2008a]. Nominally the authors show that the amplification of the electron density perturbation in the ionospheric plasma at the F-region is strongly dependent on the geomagnetic inclination. This effect is explained by the Lorenz force term in the momentum equation characterizing the neutral plasma coupling [equation (8) in *Occhipinti et al.*, 2008a]. Consequently, the detection of tsunamigenic perturbation in the F-region-plasma is more easily observed at equatorial and mid-latitude than at the high latitude. The heterogenic amplification driven by the magnetic field is not observable in the E-region; consequently, detection at low altitude by HF sounding (i.d., Doppler sounding and over-the-horizon radar) is not affected by the geographical location.

[15] Recent studies have shown several ionospheric tsunami detections in far field by GPS-derived TEC [*Rolland et al.*, 2010]. The observed ionospheric perturbation moves coherently with the tsunami at the sea level; comparison with oceanic DART data shows similarity in the waveform

as well as in the spectral signature of the ionospheric and oceanic data, proving again that ionosphere is a sensitive medium to the tsunami propagation.

[16] Particular attention has been recently paid to the Tohoku-Oki event (11 March 2011, Mw: 9.0). Thanks to the really dense GPS network in Japan (GEONET), the co-seismic TEC perturbations at the source give a clear image of the ionospheric perturbation in the near field [*Tsugawa et al.*, 2011; *Saito et al.*, 2011; *Rolland et al.*, 2011b]; including the acoustic-gravity wave generated by the vertical displacement of the source [*Astafyeva et al.*, 2011], acoustic waves coupled with Rayleigh waves as well as the gravity wave induced by the tsunami propagation [*Liu et al.*, 2011; *Galvan et al.*, 2012]. The analysis of the first arrival in the TEC data in the epicentral also allowed the localization of the epicenter with a discrepancy of less than 100 km from the official USGS localization [*Tsugawa et al.*, 2011; *Tsai et al.*, 2011; *Astafyeva et al.*, 2011].

[17] Additionally, qualitative perturbation was also observed by four ionosondes [*Liu and Sun*, 2011] as well as by the Japanese superDARN Hokkaido radar [*Nishitani et al.*, 2011] who clearly show the detection of the ionospheric signature of the Rayleigh waves as already observed in the past by the French OTH radar Nostradamus [*Occhipinti et al.*, 2010].

[18] Notwithstanding the huge amount of data and a clear image of the perturbation, the discrimination between acoustic-gravity waves ( $AGW_{epi}$ ) generated at the epicenter by the direct vertical displacement of the source rupture and the IGW coupled with the tsunami ( $IGW_{tsuna}$ ) is still difficult. As the specific high speed of Rayleigh wave (3.5 km/s), its signature is really recognizable in the ionosphere.

[19] This work introduces some theoretical bases to interpret the data and discriminate between acoustic-gravity waves in the source area ( $AGW_{epi}$ ) and gravity waves coupled with the tsunami ( $IGW_{tsuna}$ ).

[20] Following the increasing GPS coverage around the world, we focus here our attention on the detection of tsunamigenic ionospheric perturbations by GPS. With this work, we want also to push forward the debate about the role of ionospheric sounding in the early tsunami detection exploring the GPS-TEC perturbations close to the epicenter and appearing within the first hour after the rupture.

## 2. Observations and Results

[21] GPS stations located close to the epicenter are able to map co-seismic ionospheric perturbations visualizing the TEC variations [*Heki and Ping*, 2005]. Here we focus our attention on local networks SEAMARGES (number of stations: 30) and CTO/SUGAR (n.s.: 6 to 32, from 2004 to 2006) located in Sumatra; as well as the CTO/CENTRAL-ANDES (n.s.: 10), SAMOANET (n.s.: 13), and GEONET (around 1000 stations) networks, respectively, settled in Chile, Samoa Island, and Japan. All these networks performed the detection of co-seismic perturbations induced by the following tsunamigenic seismic events: the 26 December 2004 (M: 9.1) and 12 September 2007 (M: 8.5) in Sumatra, the 14 November 2007 in Chile (M: 7.7), the 29 September 2009 in Samoa (M: 8.1), and the recent Tohoku-Oki (Japan) earthquake on 11 March 2011 (Mw: 9.0). (Magnitudes from USGS: <http://earthquake.usgs.gov/>).

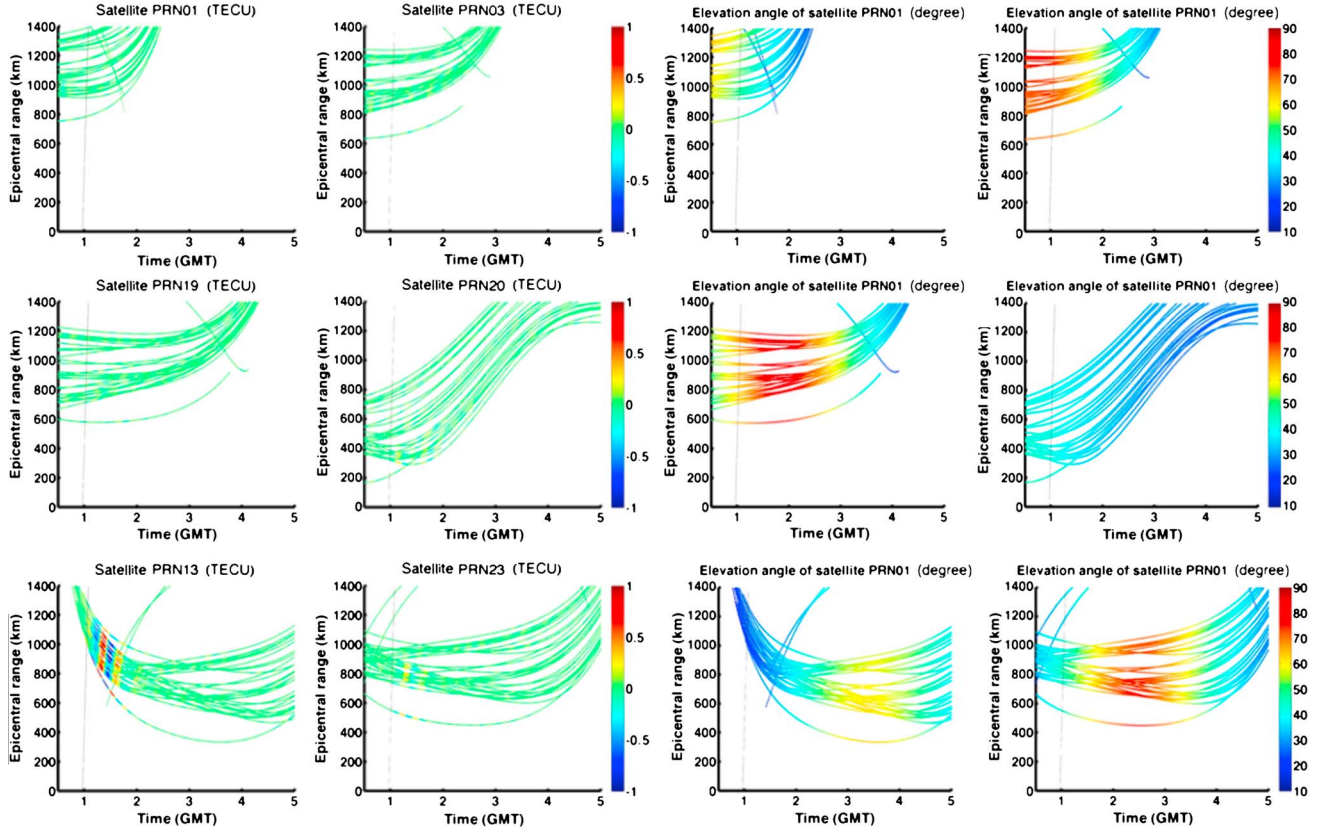


**Figure 3.** TEC perturbations from Figure 2 shown here as hodochrone (left) and with respect to the elevation angle of the satellite (right). The hodochrone refers to the epicenter and highlights the coherence of the IGW propagation from the epicenter. The elevation angle of the visible satellites clearly supports the hypothesis that low elevation improves the sensitivity to the wave structure.

[22] In order to put in evidence the signature of gravity waves induced by the tsunami generation ( $IGW_{tsuna}$ ), as well as the signature of acoustic-gravity waves induced by the vertical displacement at the source ( $AGW_{epi}$ ) and acoustic waves coupled with Rayleigh waves, all the TEC variations shown here are filtered between 1 and 8 mHz as suggested by previous observational [Artru *et al.*, 2005] and theoretical works [Lognonné *et al.*, 1998; Occhipinti *et al.*, 2008a]. A clear ionospheric perturbation appears in the TEC observations systematically within the hour after the tsunami generation, and it presents a coherent propagation from the epicenter with a horizontal speed in the order of 200–1000 m/s. This signal is linked to both, the tsunami propagation, as well as to the vertical displacement at the epicenter involved in the tsunami generation. We highlight that the effect of the source in the atmosphere/ionosphere is not affected by the presence of the water, as the displacement is directly transferred to the sea surface (incompressible hypothesis).

[23] In the case of the huge Sumatra tsunami in 2004, the 30 GPS stations of the SEAMERGES network, principally located in the Malay-peninsula and Malaysia, allow to map a large part of the overlooking ionosphere thanks to the six satellites visible on the sky (Figures 2 and 3).

[24] Figure 2 shows the ionospheric piercing points (IPPs), in essence the projection of the SEAMERGES network along the line of sight to the six satellites on the ionospheric layer corresponding to the maximum of ionization ( $\sim 300$  km). The perturbation, moving with a speed of

around 550 m/s, is visible during almost 1 h by satellites with an elevation above  $10^\circ$ .

[25] The really strong amplitude of the TEC ionospheric perturbation generated by the huge Sumatra tsunami in 2004 is not only explained by the tremendous sea-surface displacement but also by the propitious observation geometry (Figure 2). As a consequence of the integrated nature of TEC along the station-satellite line of sight, satellites at low elevation are able to better highlight the presence of an oscillating perturbation. The alternated positive and negative phases result in a close to zero integral when the satellite is close to the zenith; at the opposite, the horizontal integration reveals the presence of the perturbation. Figure 3 clearly shows this effect: the perturbation in the TEC measurements is strongly visible on the satellite PRN-13 close to  $10^\circ$  of elevation, followed by satellites PRN-23 and PRN-20 at around  $45^\circ$  of elevation. As the oscillating perturbation starts to be visible only after 15 min after the rupture, it fits with the arrival time of the acoustic-gravity wave generated by the vertical displacement of the extended source ( $AGW_{epi}$ ).

[26] Similar signals (both  $AGW_{epi}$  and  $IGW_{tsuna}$ ) are systematically observed in the ionosphere overlooking tsunamigenic epicenters. The beautiful observation following the Sumatra earthquake in 2007 (Figure 4-left) performed by the five GPS stations of the CTO/SUGAR network shows and follows the perturbation until 1000 km from the epicenter.

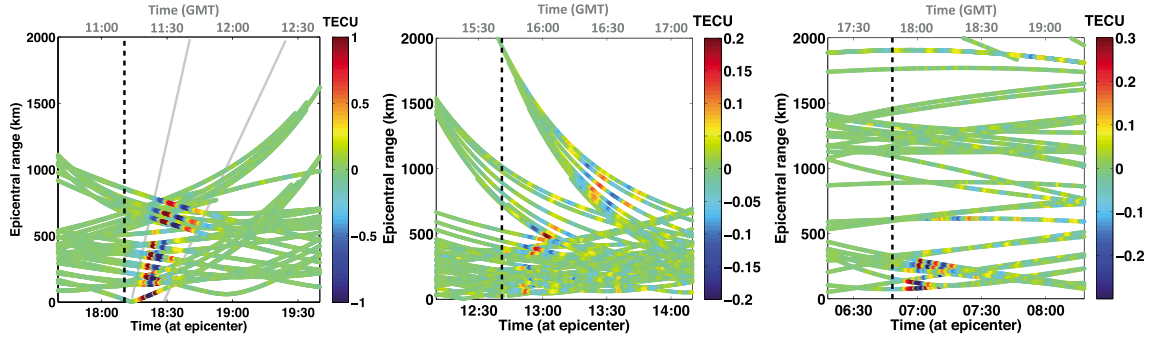


**Figure 4.** Hodochrones of the TEC perturbation (passband filtered between 1 and 8 mHz) for the following tsunamigenic seismic events: Sumatra 2007 (M: 8.5, left), Chile 2007 (M: 7.7, middle), Samoa 2009 (M: 8.1, right). Dotted lines show the event time; the two gray lines show the speed of 1000 m/s and 550 m/s. We highlight that perturbations observed during Chile 2007 and Samoa 2009 are five times and three times smaller than the perturbation observed during Sumatra 2007, respectively.

[27] We can distinguish two different components in the first wave ( $AGW_{epi}$ ): the closer one moving at the speed of the high-atmospheric acoustic waves of around 1000 m/s; the second one, slower and more similar to an acoustic-gravity wave, moving at around 550 m/s. This wave is most likely generated by the ground displacement (and the subsequent sea-surface displacement resulting in a tsunami) due to the seismic rupture, that appears as an acoustic-gravity pulse ( $AGW_{epi}$ ) and disappears within 1000 km. We highlight that a pure gravity wave generated by the tsunami ( $IGW_{tsuna}$ ) appears further on the 500 km, and it is detectable at the great distance following the tsunami during its propagation [Artru et al., 2005; Occhipinti et al., 2006, 2008b; Rolland et al., 2010; Occhipinti et al., 2011].

[28] A smaller TEC perturbation is observed after the Chile earthquake (Figure 4-center). In this case, we do not see a clear signature of the pure acoustic component but only the acoustic-gravity wave moving at around 450 m/s. The acoustic-gravity pulse ( $AGW_{epi}$ ), linked to the direct ground displacement [Rolland et al., 2011a], seems to disappear within 800 km, and it is replaced by a wave moving slower, at around 300–350 m/s. This last wave is most likely the tsunamic internal gravity wave ( $IGW_{tsuna}$ ) propagating in the atmosphere and perturbing the ionospheric plasma [Occhipinti et al., 2006, 2008a].

[29] The perturbation observed at the epicenter by the GPS SAMOANET network following the Samoa tsunami (Figure 4-right) shows a clear signature of the acoustic pulse but not evidence neither of the acoustic-gravity component of the pulse induced by the ground displacement at the epicenter, nor of the plasma perturbation induced by the tsunamic IGWs. The absence of the visible signals is probably due to the high elevation of the satellite or the scarce coverage.

[30] Anyway, for the Chile and Samoa events, the tsunami-related IGW in the ionosphere crossing the Pacific ocean are also detected by the Hawaiian GPS network at the East of Hawaii [Rolland et al., 2010]. The ionospheric measurements are coherent with the tsunami observation at the sea level performed by tide gauge located in the Hawaiian harbor and the DART buoys [Rolland et al., 2010].

[31] The last observation presented here and strongly supporting the hypothesis of the early tsunamigenic TEC perturbation detected by ionospheric sounding was performed on 11 March 2011 by the Japanese dense GPS network, GEONET, following the tsunamigenic Tohoku-Oki earthquake (Figure 5). The ionospheric perturbations induced by this tremendous event are so important that they are visible to all satellites independently of the observation geometry.

[32] The observed perturbation appears within the first 10 min after the earthquake; anyway, we highlight that previous works claim the detection of the first arrival of acoustic waves as soon as 7–8 min after the rupture [Tsugawa et al., 2011; Astafyeva et al., 2011].

[33] We observe here several waves, particularly superimposed in the epicentral area.

[34] We first notice an acoustic wave, coupled with a Rayleigh wave (Figure 5, Sat. 15 and 26), appearing after 10 min and moving horizontally at the Rayleigh wave speed (3.5 km/s). As a consequence of this really fast horizontal speed, the Rayleigh wave signature in the ionosphere is easily recognizable.

[35] Within the 20 min after the rupture, another wave appears (Figure 5). It is an acoustic-gravity wave where we clearly discriminate two components: a faster (~500–600 m/s) acoustic wave and a slower (~200–300 m/s) gravity wave.

[36] This wave seems to disappear within 1000 km from the epicenter (e.g., Sat 26, 27, 15, and 9); then, a pure gravity wave, with a speed of 200–300 m/s, continues the propagation.

[37] The spectral analysis of the Japanese TEC observations clearly shows the acoustic and gravity nature of the detected waves (Figure 6). In essence, within the first 20 min, we observe the acoustic-gravity pulse generated by the vertical displacement at the source ( $AGW_{eli}$ ); then, we observe a pure gravity wave coupled with the tsunami propagating at the sea level ( $IGW_{tsuna}$ ). We highlight that the first pulse could be used to estimate the vertical displacement of the ground producing the tsunami. In the next paragraph, we present a theoretical support to discriminate those waves.

[38] The observations presented here prove that ionospheric sounding, close to the seismic network and sea level measurements (tide gauges, DARTs, etc.), could play an important role in the oceanic monitoring and tsunami warning system.

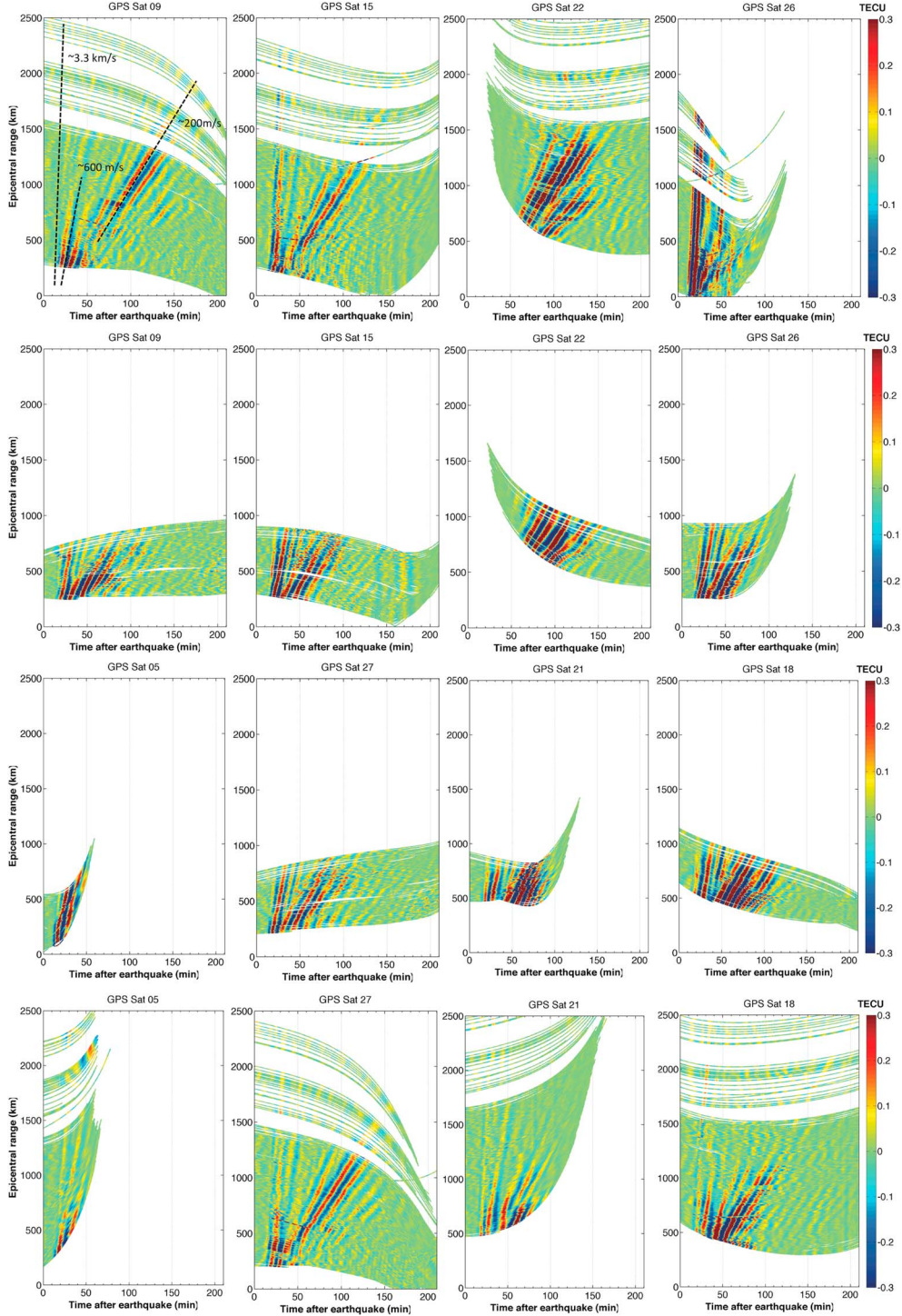


**Figure 5.** Hodochrones of the TEC perturbation observed by the Japanese GEONET network and by eight satellites (indicated in the top) following the recent Tohoku-Oki tsunamigenic earthquake (2011, M: 9.0). We observe an acoustic wave coupled with Rayleigh wave starting from the epicenter with a speed of around 3.3 km/s and a superimposed acoustic-gravity wave moving with a speed of around 650 m/s. The acoustic-gravity wave generated at the epicenter disappears after 500–1000 km, and it is replaced by a pure gravity wave coupled with the tsunami that moves with a speed of around 200 m/s. For easy reading, the TEC North (up and bottom rows) and South (middle rows) observations are separated.

### 3. Theoretical Support

[39] Tsunamis are oceanic IGWs [Satake, 2002], their frequency is generally smaller than Brünt-Väisalla frequency,

and, in the limit of linear analysis, they generate IGWs in the overlying atmosphere [Hines, 1972; Occhipinti et al., 2006, 2008a]. Forcing the bottom boundary of the atmosphere, the tsunami transfers in the atmosphere its horizontal k-number

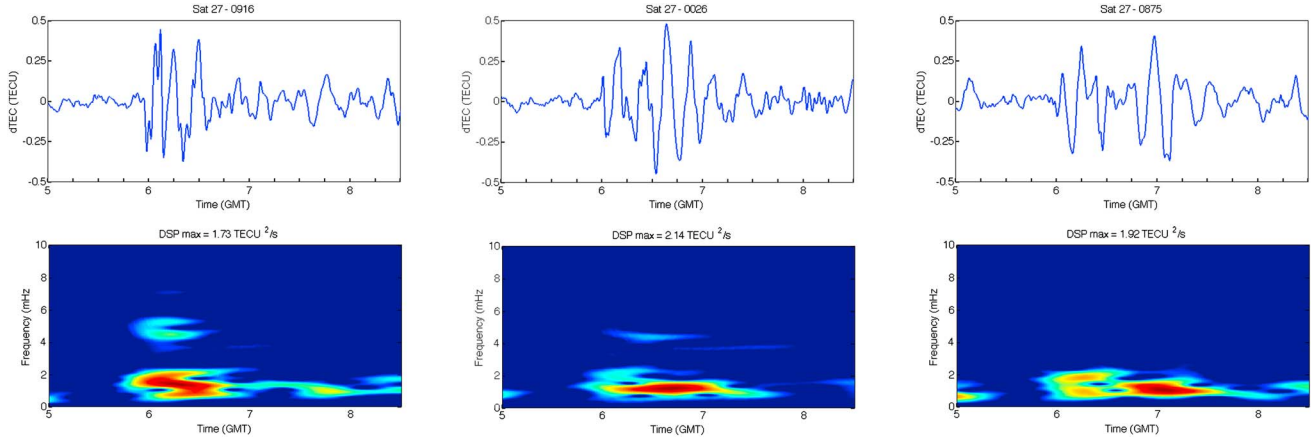


**Figure 6.** TEC perturbations (top) and spectral analysis (bottom) of three station-satellite couples of the Japanese GEONET network after the Tohoku-Oki tsunamigenic earthquake (2011, Mw 9). Also, here we observe an acoustic-gravity wave appearing within 20 min after the rupture (left and middle panels) and a pure gravity wave appearing in a far field (after 500 km, middle and right panels). We remind that the Brünt-Vaisalla frequency (limit between acoustic and gravity domain) is in the order of 3 mHz.

$k_h$ , its period  $T$ , and consequently its horizontal phase speed  $v_{tsuna} = \sqrt{gH}$ ; where  $g$  is the gravity acceleration and  $H$  is the ocean depth. We note that the  $k$ -vector  $k_h$ , the period  $T$ , and the horizontal phase speed  $v_{tsuna}$  are constant during the upward propagation of the tsunamigenic internal gravity wave (IGW<sub>tsuna</sub>).

[40] Following *Occhipinti et al.* [2008a], in the case of linearized theory for a realistic atmosphere with horizontal stratification and no-background wind, the vertical  $k$ -number  $k_z$  takes the form (1) and consequently the dispersion equation the form (2).

$$k_z = \sqrt{k_h^2 \left( \frac{N^2}{\omega^2} - 1 \right) - \left( \frac{N^2}{2g} \right)^2} \quad (1)$$

$$\omega^2 = \frac{k_h^2 N^2}{k_z^2 + k_h^2 + \left( \frac{N^2}{2g} \right)^2} \quad (2)$$

[41] In order to estimate the vertical propagation delay that the tsunami-driven IGWs spend to reach the ionosphere, we evaluate the vertical and horizontal group velocity  $v_g^z$  and  $v_g^h$  (Figure 7):

$$v_g^h = \frac{\partial \omega}{\partial k_h} = \frac{k_h N^2 (D - k_h^2)}{\omega D^2} \quad v_g^z = \frac{\partial \omega}{\partial k_z} = -\frac{k_z k_h^2 N^2}{\omega D^2}$$

where  $D = k_z^2 + k_h^2 + \left( \frac{N^2}{2g} \right)^2$  is the denominator of the dispersion equation (2).

[42] We highlight first, that the vertical group velocity  $v_g^z$  has an inverted sign compared to the vertical phase velocity ( $\omega/k_z$ ). This is a typical propagation condition of IGWs as the atmosphere falls down by the effect of the gravity; consequently, the vertical phase velocity is negative, and the vertical group velocity is positive, generating an upward propagation of the IGW. We also highlight that if the horizontal phase velocity of the atmospheric gravity wave is the same as the tsunami ones ( $\omega/k_h = v_{tsuna} = \sqrt{gH}$ ), this is not anymore the case for the group velocity, which is

furthermore dispersive, which was not the case for tsunami where group and phase velocity are the same. The horizontal group velocity of the generated IGW is always smaller than the horizontal phase velocity (Figure 7). The horizontal group velocity does not play a role in the vertical propagation delay, but it is useful to estimate the epicentral distance where the IGWs start to interact with the ionosphere as well as the delay  $\delta t$  between the tsunami propagating at the sea surface and the IGW propagating in the atmosphere at the altitude  $z_{iono}$  (Figure 8).

$$\delta t = \frac{1}{v_{tsuna}} \int_0^{z_{iono}} \frac{v_{tsuna} - v_g^h(z)}{v_g^z(z)} dz$$

[43] The delay  $\delta t$  is usually mishandled in many observational papers [e.g., *Liu et al.*, 2006b] as the IGW is interpreted as a pure vertical wave. Consequently, the observed delay  $\delta t$  is explained only by the vertical velocity resulting in a wrong overestimation. Observing a delay  $\delta t$  of around 8 min, *Liu et al.* [2006b] estimate a vertical velocity of 730 m/s incompatible with the theoretical tsunami-induced IGW vertical velocity (Figure 7).

[44] The delay  $\delta t$  shown in Figure 8 is computed with the hypothesis that  $v_{tsuna}$  is not changing, e.g., during the tsunami propagation offshore. Consequently, the delay  $\delta t$  is always positive, and the tsunami at the sea surface arrives always before the IGW<sub>tsuna</sub>. This is not the case when the tsunami reaches the coasts: there, the tsunami at the sea surface reduces its speed  $v_{tsuna}$ , and the IGW<sub>tsuna</sub>, conserving the same its horizontal speed, can go beyond the tsunami wavefront. This phenomenon was clearly observed and described by G. Occhipinti et al. submitted (2011) during the Tohoku event, when the tsunami reached the Hawaiian coasts.

[45] Figure 7 clearly shows the structure of the atmosphere in the group velocity behavior with particular attention to the presence of the thermopause ( $\approx 125$  km) where we observe a strong acceleration and deceleration in the vertical and

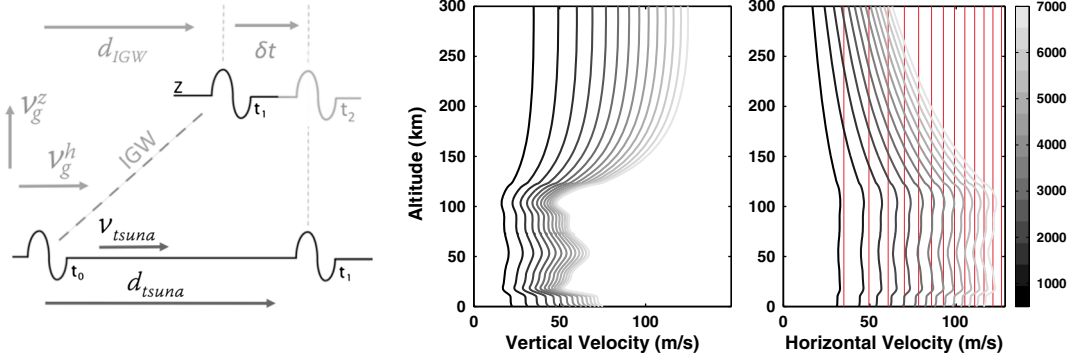


**Figure 7.** Schematic description of the propagation of internal gravity wave (IGW) coupled with the tsunami (left): as the tsunami speed  $v_{tsuna}$  is always bigger than the horizontal group velocity ( $v_g^h$ ) of the IGW, there is always an observational delay  $\delta t$  (see Figure 8) between the IGW at the altitude  $z$  and the tsunami at the sea level. The vertical ( $v_g^z$ ) and the horizontal ( $v_g^h$ ) group velocity of the internal gravity wave coupled at the sea surface with tsunamis, generated at different oceanic deep  $h$  (m), see gray scale, and a characteristic period  $T$  of 10 min, are shown in the center and right plot, respectively. Tsunamis move at the speed defined by the relation  $v_{tsuna} = \sqrt{hg}$  (red line in the right plot), where  $g$  is the gravity acceleration. Consequently, the horizontal  $k$ -vector  $k_h$  that the tsunami transfer to the atmospheric internal gravity wave also depends by  $h$  following the relation  $k_h = \frac{2\pi}{T\sqrt{hg}}$ . Note that tsunamis generated/moving in the deeper oceanic zone produce faster IGW. The  $d_{tsuna}$  and  $d_{IGW}$  represent the horizontal distances covered by the tsunami and the IGW, respectively (see Figure 8).

horizontal propagations, respectively. This means that until the thermopause, the IGW closely follows the tsunami during its horizontal propagation.

[46] Based on the vertical velocity  $v_g^z$  shown in Figure 7, the resulting theoretical delay to reach the maximum of ionization in the ionosphere ( $\approx 300$  km) is on the order of 60 min for a tsunami generated in a deep ocean of 7000 m; the vertical delay becomes longer for a tsunami in a low-deep ocean (Figure 8). We highlight that this delay is coherent with the observation of the wave changing (Figures 4 and 5), where we start to observe the IGW coupled with the tsunami.

[47] The epicentral distance where the IGW starts to interact with the ionospheric plasma is in the order of 400 km for the E-region and 600 km for the F-region (Figure 8). This epicentral distance is coherent with the observations presented here, where we highlight the presence of the IGW after 500 km (Figures 3, 4, and 5).

[48] We remind that the perturbations ( $AGW_{epi}$ ) observed closer to the epicenter ( $<500$  km) are at higher frequency and move faster compared to the tsunami-related perturbations.

[49] Indeed, the coupling mechanism ground/ocean/atmosphere/ionosphere close to the epicenter is more complex as plenty of phenomena appear superimposed in that region:

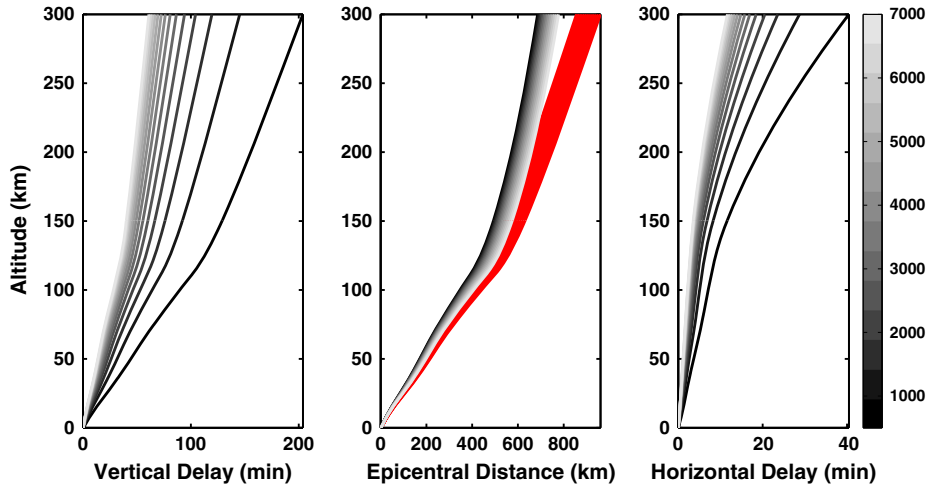


**Figure 8.** Vertical propagation delay (left) of the internal gravity wave (IGW) coupled at the sea surface with tsunamis (generated at different oceanic depth  $h$  (m), see gray scale, and with a characteristic period  $T$  of 10 min). Middle: epicentral distances ( $d_{tsuna}$  and  $d_{IGW}$ , Figure 7) covered by the tsunami (red) and the coupled IGW (gray scale) during the delay spent by the IGW to reach the altitude shown in the y axis. Right: horizontal delay  $\delta t$  between the tsunami at the sea level and the coupled IGW at fixed altitudes (time to cross the same zenith).

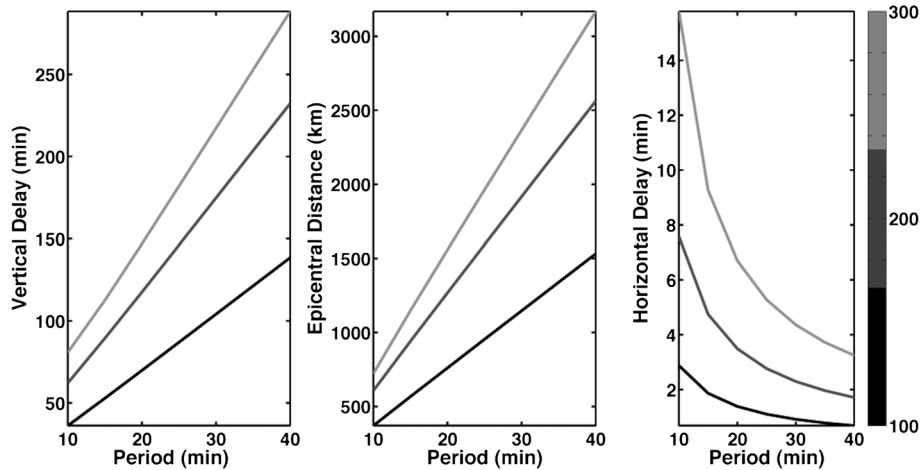


**Figure 9.** Period dependence of the (left) vertical propagation delay, (middle) epicentral distance, and (right) horizontal delay between the tsunami at the sea level and the coupled IGW. This figure generalizes the period dependence of the result shown in Figure 8. The color scale shows the different altitudes reached by the IGW, nominally 100, 200, and 300 km. The minimum detection time delay of the IGW with GPS-TEC is 40 min, corresponding to a minimum of 450 km of epicentral distance and 3 min behind the tsunami at sea level for an IGW reaching the low ionosphere at 100 km and a period of 10 min.

[50] 1. First, a reproducible signature in the ionospheric at  $\sim 3\text{--}5$  mHz moving horizontally at  $\sim 3.5$  km/s is induced by the generation and propagation of Rayleigh waves, and it is already observed by TEC-GPS [Ducic *et al.*, 2003; Rolland *et al.*, 2011a], Doppler sounding [Artru *et al.*, 2004; Occhipinti *et al.*, 2010] as well as OTH radar [Occhipinti *et al.*, 2010]. This perturbation, induced by the ground vertical displacement induced by surface waves, allows to image the radiation pattern of the seismic tensor in the near field [Rolland *et al.*, 2011a], and it is routinely observed by Doppler sounders in the far field for earthquakes with a magnitude bigger than 6.5 [Artru *et al.*, 2004].

[51] 2. Second, an acoustic-gravity pulse (generated at the source by the rapid rupture displacement) is the less understood because of the complexity of the seismic rupture. Several papers measure it in the ionosphere [Afrimovich *et al.*, 2001; Astafyeva and Heki, 2009; Astafyeva *et al.*, 2009; Rolland *et al.*, 2011b; Astafyeva *et al.*, 2011], but no forward modeling is today able to clearly reproduce it.

[52] 3. Last, during tsunamigenic earthquakes, a component of the ionospheric perturbation is induced by the propagation of IGW forced by the tsunami in the overlooking atmosphere. The offshore perturbation has already been observed [Artru *et al.*, 2005; Occhipinti *et al.*, 2006, 2008b; Rolland *et al.*, 2010; [Makela *et al.*, 2011; Occhipinti *et al.*, 2011] and reproduced [Occhipinti *et al.*, 2006, Occhipinti *et al.*, 2011].

[53] The theoretical results shown in this section introduce some constraints to the gravity waves appearing in the ionosphere and forced at the sea level by the tsunami propagation (iii). In essence, the tsunami signature in the ionosphere can be visible at least at around 500 km from the epicenter between 25 and mainly 60 min, corresponding at the time to reach ionosphere at its base (100 km) and at the maximum of ionization (300 km), respectively. Once the perturbation is visible in the ionosphere, the delay between the tsunami at the sea level and the perturbation in the ionosphere can be

estimated at around 10–15 min for a tsunami with a main period of around 10 min (Figure 8). We highlight that this delay is reduced at few minutes for tsunami with a main period longer than 10 min (Figure 9).

#### 4. Conclusion

[54] Tsunamigenic earthquakes are first detected and estimated by seismic networks in order to define the magnitude and the source geometry and localize the epicenter in order to state the tsunami risk. After this first step, the tsunami risk is usually validated by the sea level measurements (tide gauges, DARTs, etc.). This second validation can take several hours before that the tsunami reach the buoys, sparsely located around the oceans, and the tsunami signal is recorded for filtering purposes. In this study, we present a series of ionospheric observations induced by tsunami-generated IGWs appearing within the first hour after the rupture and at around 500 km from the epicenter ( $IGW_{tsuna}$ ).

[55] We also highlight the presence of ionospheric perturbations linked to acoustic-gravity waves directly generated by the vertical displacement induced by the rupture ( $AGW_{epi}$ ). Notwithstanding this perturbation is not clearly explained by numerical modeling, the vertical displacement is also involved in the tsunami genesis and could be used to estimate the amplitude of the tsunami.

[56] Despite the estimation of the sea-surface displacement *via* the ionospheric sounding is not immediate because of the modulation of the TEC amplitude introduced by the magnetic field [Occhipinti *et al.*, 2008a], and because the effect of observational geometry (showed in this study), the tsunami detection by ionospheric monitoring has the potential to support classic techniques for tsunami monitoring.

[57] Particularly in the far field, where the tsunami at the sea level and its signature in the ionosphere move together with an observational delay between few minutes to 15 min

(depending of the main tsunami period), the tsunami can be easily detected and tracked by ionospheric monitoring.

[58] With this work, we wish to encourage the use of ionospheric monitoring as a potential support for future oceanic monitoring and tsunami warning systems.

[59] **Acknowledgments.** This project is supported by CNES, ANR TO-EOS, and PNTS programs. It started during the visiting of S.W. at the IPGP and was finalized during the visiting of G.O. at the ERI; consequently, G.O. and S.W. strongly thank the IPGP and ERI visiting programs for support. L.R. is supported by funding of the University of Nice. The GPS data used in this work are supplied by different local GPS networks that we strongly thank: the SEAMARGES GPS network in South-East Asian; the Caltech Tectonic Observatory SUGAR and CENTRAL-ANDES networks, respectively, located in Sumatra and Chile; the SAMOANET network and the Hawaiian GPS network, respectively, located in Samoa and Hawaii. We strongly thank people working on networks and database to make science ambitious. Thanks are extended to the different national agencies (Department of Survey and Mapping Malaysia (DSMM), Royal Thai Survey Department (RTSD), and Indonesian National Agency for Survey and Mapping (BAKOSURTANAL)) for sharing their regional GPS data in the framework of the SEAMERGES (<http://www.deos.tudelft.nl/seamerges>) project, described in Vigny et al. [2005]. SEAMERGES has been funded by the ASEAN-EU University Network Program (AUNP). We also thank M. Hashizume for contributing Thai data collected by Chulalongkorn University in cooperation with the Frontier Observational Research System for Global Change (FRONTIER) project and the Earthquake Research Institute at the University of Tokyo. G.O. thanks J.-P. Avouac (Caltech Tectonic Observatory) for friendly and constructive discussions, as well as Caroline Journaux for the cartoon on Figure 1.

[60] We thank three anonymous reviewers for their constructive remarks. This is IPGP contribution 3397.

## References

Afraimovich, E. L., N. P. Perevalova, A. V. Plotnikov, and A. M. Uralov (2001), The shock-acoustic waves generated by earthquakes, *Ann. Geophys.*, *19*, 395–409.

Afraimovich, E. L., N. P. Perevalova, and S. V. Voyeikov (2003), Traveling wave packets of total electron content disturbances as deduced from GPS network data, *J. Atmos. Sol. Terr. Phys.*, *65*, 1245–1262.

Ammon, C. J., A. A. Velasco, and T. Lay (2006), Rapid estimation of first-order rupture characteristics for large earthquakes using surface waves: 2004 Sumatra-Andaman earthquake, *Geophys. Res. Lett.*, *33*, L14314, doi:10.1029/2006GL026303.

Artru, J., T. Farges, and P. Lognonné (2004), Acoustic waves generated from seismic surface waves: propagation properties determined from Doppler sounding and normal-mode modeling, *Geophys. J. Int.*, *158*(3), 1067–1077.

Artru, J., V. Ducic, H. Kanamori, P. Lognonné, and M. Murakami (2005), Ionospheric detection of gravity waves induced by tsunamis, *J. Geophys. Res.*, *160*, doi:10.1111/j.1365-246X.2005.02552.x.

Astafeyeva, E., and K. Heki (2009), Dependence of waveform of near-field coseismic ionospheric disturbances on focal mechanisms, *Earth Planets Space*, *61*, 939–943.

Astafeyeva, E., K. Heki, V. Kiryushkin, E. Afraimovich, and S. Shalimov (2009), Two-mode long-distance propagation of coseismic ionosphere disturbances, *J. Geophys. Res.*, *114*, A10307, doi:10.1029/2008JA013853.

Astafeyeva, E., P. Lognonné, and L. Rolland (2011), First ionosphere images for the seismic slip of the Tohoku-oki Earthquake, *Geophys. Res. Lett.*, *38*, L22104, doi:10.1029/2011GL049623.

Balasis, G., and M. Manda (2007), Can electromagnetic disturbances related to the recent great earthquakes be detected by satellite magnetometers?, *Tectonophysics*, *431*, 173–195 p., doi:10.1016/j.tecto.2006.05.038.

Balthazor, R. L., and R. J. Moffett (1997), A study of atmospheric gravity waves and travelling ionospheric disturbances at equatorial latitudes, *Ann. Geophys.*, *15*, 1048–1056.

Bilitza, D., C. Koblinsky, S. Zia, R. Williamson, and B. Beckley (1996), The equator anomaly region as seen by the TOPEX/Poseidon satellite, *Adv. Space Res.*, *18*(6), 23–32.

Coisson, P., G. Occhipinti, P. Lognonné, and L. M. Rolland (2011), Tsunami signature in the ionosphere: the innovative role of OTH radar, *Radio Sci.*, *46*, RS0D20, doi:10.1029/2010RS004603.

DasGupta, A., A. Das, D. Hui, K. K. Bandyopadhyay, and M. R. Sivaraman (2006), Ionospheric perturbation observed by the GPS following the December 26th, 2004 Sumatra-Andaman earthquake, *Earth Planet. Space*, *35*, 929–959.

Ducic, V., J. Artru, and P. Lognonné (2003), Ionospheric remote sensing of the Denali Earthquake Rayleigh surface waves, *Geophys. Res. Lett.*, *30*(18), 1951, doi:10.1029/2003GL017812.

Galvan, D. A., A. Komjathy, M. P. Hickey, P. Stephens, J. Snively, Y. T. Song, M. D. Butala, and A. J. Mannucci (2012), Ionospheric signatures of Tohoku-Oki tsunamis of March 11, 2011: Model comparisons near the epicenter, *Radio Sci.*, *47*, 4003, doi:10.1029/2012RS005023.

Garcia, R., F. Crespon, V. Ducic, and P. Lognonné (2005), 3D Ionospheric tomography of post-seismic perturbations produced by Denali earthquake from GPS data, *Geophys. J. Int.*, *163*, 1049–1064, doi:10.1111/j.1365-246X.2005.02775.x.

Gonzalez, F. I., E. N. Bernard, C. Meinig, M. C. Eble, H. O. Mofjeld, and S. Stalin (2005), The NTHMP Tsunameter Network, *Nat. Hazards*, *35*, 25–39.

Heki, K., and J. Ping (2005), Directivity and apparent velocity of the coseismic traveling ionospheric disturbances observed with a dense GPS network, *Earth Planet. Sci. Lett.*, *236*, 845–855.

Hickey, M. P., G. Schubert, and R. L. Walterscheid (2009), The Propagation of Tsunami-Driven Gravity Waves into the Thermosphere and Ionosphere, *J. Geophys. Res.*, *114*, A08304, doi:10.1029/2009JA014105.

Hickey, M. P., G. Schubert, and R. L. Walterscheid (2010), Atmospheric airglow fluctuations due to a tsunami-driven gravity wave disturbance, *J. Geophys. Res.*, *115*, A06308, doi:10.1029/2009JA014977.

Hines, C. O. (1972), Gravity waves in the atmosphere, *Nature*, *239*, 73–78.

Iyemori, T., et al. (2005), Geomagnetic pulsations caused by the Sumatra earthquake on December 26, 2004, *Geophys. Res. Lett.*, *32*, L20807, doi:10.1029/2005GL024083.

Lay, T., et al. (2005), The great Sumatra-Andaman earthquake of 26 December 2004, *Science*, *308*, 1127–1133.

Le Pichon, A., P. Herry, P. Mialle, J. Vergoz, N. Brachet, M. Garces, D. Drob, and L. Ceranna (2005), Infrasound associated with 2004–2005 large Sumatra earthquakes and tsunami, *Geophys. Res. Lett.*, *32*, L19802, doi:10.1029/2005GL023893.

Liu, J.-Y., and Y.-Y. Sun (2011), Seismo-traveling ionospheric disturbances of ionograms observed during the 2011 Mw 9.0 Tohoku Earthquake, *Earth Planets Space*, *63*, 897–902.

Liu, J. Y., Y. B. Tsai, S. W. Chen, C. P. Lee, Y. C. Chen, H. Y. Yen, W. Y. Chang, and C. Liu (2006a), Giant ionospheric disturbances excited by the M9.3 Sumatra earthquake of 26 December 2004, *Geophys. Res. Lett.*, *33*, L02103, doi:10.1029/2005GL023963.

Liu, J., Y. Tsai, K. Ma, Y. Chen, H. Tsai, C. Lin, M. Kamogawa, and C. Lee (2006b), Ionospheric GPS total electron content (TEC) disturbances triggered by the 26 December 2004 Indian Ocean tsunami, *J. Geophys. Res.*, *111*, A05303, doi:10.1029/2005JA011200.

Liu, J.-Y., C.-H. Chen, C.-H. Lin, H.-F. Tsai, C.-H. Chen, and M. Kamogawa (2011), Ionospheric disturbances triggered by the 11 March 2011 M9.0 Tohoku earthquake, *J. Geophys. Res.*, *116*, A06319, doi:10.1029/2011JA016761.

Lognonné, P., E. Clévéde, and H. Kanamori (1998), Computation of seismograms and atmospheric oscillations by normal-mode summation for a spherical Earth model with realistic atmosphere, *Geophys. J. Int.*, *135*, 388–406.

Lognonné, P., J. R. Artru, F. Garcia, V. Crespon, E. Ducic, G. Jeansou, J. Occhipinti, G. Helbert, G. Moreaux, and P. E. Godet (2006), Ground based GPS imaging of ionospheric post-seismic signal, *Planet. Space Sci.*, *54*, 528–540.

Mai, C.-L., and J.-F. Kiang (2009), Modeling of ionospheric perturbation by 2004 Sumatra tsunami, *Radio Sci.*, *44*, RS3011, doi:10.1029/2008RS004060.

Makela, J. J. et al. (2011), Imaging and modelling the ionospheric response to the 11 March 2011 Sendai Tsunami over Hawaii, *Geophys. Res. Lett.*, *38*, L20807, doi:10.1029/2011GL047860.

Marghany, M., and M. Hashim (2011), 3D tsunami wave reconstruction from Quicbird data by using fuzzy B-spline, *Int. J. Phys. Sci.*, *6*(13), 3111–3115.

Nishitani, N., T. Ogawa, Y. Otsuka, K. Hosokawa, and T. Hori (2011), Propagation of large amplitude ionospheric disturbances with velocity dispersion observed by the SuperDARN Hokkaido radar after the 2011 off the Pacific coast of Tohoku Earthquake, *Earth Planets Space*, *63*, 891–896.

Occhipinti, G., P. Lognonné, E. Alam Kherani, and H. Hebert (2006), Three-dimensional waveform modeling of ionospheric signature induced by the 2004 Sumatra tsunami, *Geophys. Res. Lett.*, *33*, L20104, doi:10.1029/2006GL026865.

Occhipinti, G., P. Lognonné, E. Alam Kherani, and H. Hebert (2006), Three-dimensional waveform modeling of ionospheric signature induced by the 2004 Sumatra tsunami, *Geophys. Res. Lett.*, *33*, L20104, doi:10.1029/2006GL026865.

Occhipinti, G., E. Alam Kherani, and P. Lognonné (2008a), Geomagnetic dependence of ionospheric disturbances induced by tsunamigenic internal gravity waves, *Geophys. J. Int.*, doi:10.1111/j.1365-246X.2008.03760.x.

- Occhipinti, G., A. Komjathy, and P. Lognonné (2008b), Tsunami detection by GPS: how ionospheric observation might improve the Global Warning System, *GPS World*, *19*(2), 50–56.
- Occhipinti, G., P. Dorey, T. Farges, and P. Lognonné (2010), Nostradamus: The radar that wanted to be a seismometer, *Geophys. Res. Lett.*, *37*, L18104, doi:10.1029/2010GL044009.
- Occhipinti, G., P. Coisson, J. J. Makela, S. Allgeyer, A. Kherani, H. Hébert, and P. Lognonné (2011), Three-dimensional numerical modeling of tsunami-related internal gravity waves in the Hawaiian atmosphere, *Earth Planet. Sci.*, *63*, 847–851, doi:10.5047/eps.2011.06.051.
- Okal, E. A., A. Piatanesi, and P. Heinrich (1999), Tsunami detection by satellite altimetry, *J. Geophys. Res.*, *104*, 599–615.
- Park, J., K. Anderson, R. Aster, R. Butler, T. Lay, and D. Simpson (2005), Global Seismographic Network records the Great Sumatra-Andaman earthquake, *Eos. Trans. AGU*, *86*(6), 60.
- Peltier, W. R., and C. O. Hines (1976), On the possible detection of tsunamis by a monitoring of the ionosphere, *J. Geophys. Res.*, *81*, 12.
- Rolland, L., G. Occhipinti, and P. Lognonné (2010), A. Loevenbruck, The 29 September 2009 Samoan tsunami in the ionosphere detected offshore Hawaii, *Geophys. Res. Lett.*, *37*, L17191, doi:10.1029/2010GL044479.
- Rolland L. M., Lognonné P., and Munekane H. (2011a), Detection and modeling of Rayleigh waves induced patterns in the ionosphere, *J. Geophys. Res.*, *116*, A05320, doi:10.1029/2010JA016060.
- Rolland, L. M., P. Lognonné, E. Astafyeva, E. A. Kherani, N. Kobayashi, M. Mann, and H. Munekane (2011b), The resonant response of the ionosphere imaged after the 2011 off the Pacific coast of Tohoku Earthquake, *Earth Planets Space*, *63*, 853–857.
- Saito, A., T. Tsugawa, Y. Otsuka, M. Nishioka, T. Iyemori, M. Matsumura, S. Saito, C. H. Chen, Y. Goi, and N. Choosakul (2011), Acoustic resonance and plasma depletion detected by GPS total electron content observation after the 2011 off the Pacific coast of Tohoku Earthquake, *Earth Planets Space*, *63*, 863–867.
- Satake, K. (2002), Tsunamis, in *International Geophysics Series*, *81A*, edited by W. H. K. Lee, H. Kanamori, P. C. Jennings, and C. Kisslinger, pp. 437–451, Academic Press, San Diego, Calif.
- Smith, W., R. Scharroo, V. Titov, D. Arcas, and B. Arbic (2005), Satellite altimeters measure Tsunami, *Oceanography*, *18*(2), 102.
- Song, Y. T., C. Ji, L.-L. Fu, V. Zlotnicki, C. K. Shum, Y. Yi, and V. Hjorleifsdottir (2005), The 26 December 2004 tsunami source estimated from satellite radar altimetry and seismic waves, *Geophys. Res. Lett.*, *32*, L20601, doi:10.1029/2005GL023683.
- Tsai, H. F., J.-Y. Liu, C.-H. Lin, and C.-H. Chen (2011), Tracking the epicenter and the tsunami origin with GPS ionosphere observation, *Earth Planets Space*, *63*, 859–862.
- Tsugawa, T., A. Saito, Y. Otsuka, M. Nishioka, T. Maruyama, H. Kato, T. Nagatsuma, and K. T. Murata (2011), Ionospheric disturbances detected by GPS total electron content observation after the 2011 off the Pacific coast of Tohoku Earthquake, *Earth Planets Space*, *63*, 875–879.
- Vigny, C., et al. (2005), Insight into the 2004 Sumatra-Andaman earthquake from GPS measurement in southeast Asia, *Nature*, *436*, 201–206.